IEEE Access
Multidisciplinary | Rapid Review | Open Access Journal

Received October 31, 2021, accepted November 15, 2021, date of publication November 16, 2021,
date of current version November 23, 2021.

Digital Object Identifier 10.1109/ACCESS.2021.3128668

Electrochemical Immunosensor Platform Using Low-Cost ENIG PCB Finish Electrodes: Application for SARS-CoV-2 Spike Protein Sensing

RUCHIRA NANDESHWAR[1], M. SANTHOSH KUMAR[2], KIRAN KONDABAGIL[2], AND SIDDHARTH TALLUR[1]

[1]Department of Electrical Engineering, Indian Institute of Technology (IIT) Bombay, Mumbai 400076, India
[2]Department of Biosciences and Bioengineering, Indian Institute of Technology (IIT) Bombay, Mumbai 400076, India

Corresponding author: Siddharth Tallur (stallur@ee.iitb.ac.in)

The Ph.D. scholarship for Ruchira Nandeshwar is supported by the Ministry of Education (formerly Ministry of Human Resource Development), Government of India. The Ph.D. scholarship for M. Santhosh Kumar is supported by the Council of Scientific and Industrial Research (CSIR) University Grants Commission (UGC), Ministry of Education (formerly Ministry of Human Resource Development), Government of India.

ABSTRACT In recent years, lab-on-chip systems based on printed circuit board (PCB) substrates are gaining attraction primarily due to their low cost of manufacturing. Adapting inexpensive PCBs for development of immunosensors usually requires additional processing steps such as gold electroplating and electropolymerisation, that add to the manufacturing costs. In this work, we demonstrate methods to leverage electroless nickel immersion gold (ENIG) finish PCBs as electrodes for developing electrochemical immunosensors. We evaluated the performance of various parameters that impact sensor performance such as methods to clean impurities on PCB surface, optimization of redox probe concentration, and have successfully immobilized antibodies on the electrodes with cysteamine + glutaraldehyde aided process. Based on these methods, we demonstrate an application of ENIG finish PCB electrodes for detection of SARS-CoV-2 spike protein spiked in artificial saliva samples.

INDEX TERMS ENIG PCB, immunosensor, functionalization, SARS-CoV-2, spike protein.

I. INTRODUCTION

Lab-on-chip micro total analysis systems (μTAS) offer several advantages such as cost-effective chip design, miniaturized sample collection and handling and fast analysis time. The use of printed circuit boards (PCBs) has been explored for μTAS platforms since early-1990s, however integration strategies continue to be under constant development [1]. In recent times the cost of μTAS platforms has emerged as a significant technology driver, and therefore lab-on-PCB platforms are seeing renewed interest in the broad biosensors community [2]–[6]. However screen printed electrodes (SPEs) remain popular substrate choices for low-cost biosensor platforms, mainly due to challenges associated with impact of PCB gold surface roughness on reliability of immobilization of biorecognition element and the need for additional processing steps such as hard gold electroplating to prevent corrosion of underlying copper tracks on the PCB [7], [8]. SPEs utilise a variety of substrates and processes for surface modification for biosensing [9]. However, lab-on-PCB systems facilitate seamless interfacing with processing electronics. Among various type of surface finish options available for PCBs [10], the hard gold electroplating process is widely used for lab-on-PCB biosensors despite being very expensive, due to protection against corrosion offered by the thicker gold film on copper-nickel PCB tracks. Additional benefits of hard gold finish include larger electroactive surface area and reduction of pinholes, thus improving sensitivity and reliability of the sensors [11], [12]. Reports of low-cost processes such as electroless nickel immersion gold (ENIG) finish PCB electrodes utilized for biosensors employ additional gold electroplating or electropolymerization [7], [11], [13].

Gold SPEs require chemical post-processing steps to clean the impurities deposited during electroplating and to make the gold surface more electroactive [11], [14], [15]. In recent years, self assembled monolayers (SAMs) have gained a lot of attention in the field of nanotechnology, biosensors and

The associate editor coordinating the review of this manuscript and approving it for publication was Abhishek K. Jha.

bioelectronics. SAMs are formed by spontaneous absorption of the molecular constituents of the solution due to their higher affinity to a particular surface [16]. Compounds with sulfur groups (alkane thiols, disulphide) such as cystamine, 4-aminothiophenol etc. can form thiol linkages with gold surfaces to form a SAM that is used to bind organic molecules on the electrode surface [17]–[19]. Formation of SAM with cysteamine on electroplated gold electrodes have been reported in various studies [20]–[22]. There are a few studies available in literature that discuss the importance of surface properties and processing required to employ commercially available hard gold PCBs for biosensing [7], [23]. However, to the best of our knowledge, there are no such reported methods for making ENIG finish PCB electrodes more electroactive. With suitable development, the gold surface in ENIG finish PCBs does offer protection against corrosion [24]. However, surface preparation strategies to create biosensors, especially immunosensors, with ENIG finish PCBs used directly as substrate for functionalization remain unexplored.

Recently, we demonstrated the utility of low-cost ENIG finish PCB electrodes (approximately USD $0.55 per electrode when manufactured in 100 quantity) for DNA sensing, through adsorption of DNA-methylene blue intercalated complex on unprocessed PCBs [25]. In this work, we demonstrate a method to prepare electroactive ENIG finish PCB electrodes with immobilized biorecognition elements, and report strategies to clean the electrode surface, preparation of optimal redox probe concentration to avoid electrode corrosion and achieve high sensitivity. As an example of a practical application, we demonstrate detection of SARS-CoV-2 spike protein in phosphate buffer saline and in artificial saliva samples using these electrodes. The sensor utilizes antigen-antibody binding that is detected via change in voltammetric measurements performed using a low-cost smartphone compatible potentiostat. The antibodies are immobilized on the ENIG finish gold surface using cysteamine and glutaraldehyde. Detection of SARS-CoV-2 spike protein in artificial saliva is successfully achieved using differential pulse voltammetry for a wide range of antigen concentration varying from 0.1 ng/ml to 500 ng/ml. Our contribution provides a potential platform for development of low-cost point of care (POC) diagnostic and screening tool of immediate relevance in the ongoing pandemic, and complements the sensor innovations based on other platforms that have been reported in the past year and a half for this application [26]–[37]. Figure 1 shows a graphical illustration of the use case enabled by such a sensor. The underlying technology could also be readily re-purposed for other applications or pathogens, by immobilizing appropriate alternate biorecognition elements onto the electrode surface.

II. METHODS

A. MATERIALS

Artificial saliva (SAE0149), cysteamine (M9768), glutaraldehyde (G6257), bovine serum albumin (BSA) (A9085) and Ag/AgCl (60/40) screen printing paste (901773) are purchased from Sigma Aldrich. Potassium ferrocyanide ($K_4[Fe(CN)6].3H_2O$) and potassium ferricyanide ($K_3Fe(CN)_6$) are used as redox probes. Ammonium hydroxide (30 % NH_4OH) is purchased from Vetec and hydrogen peroxide (30 % H_2O_2), 2-propanol (isopropyl alcohol, IPA), acetone are purchased from EMPARTA. Ethanol (absolute, analytical grade) is purchased from Changshu Hongsheng Fine Chemical Co. Ltd. SARS-CoV-2 recombinant spike protein (Fapon Biotech Inc. catalog ID FPZ0537; 330-554 aa, 30 kDa) and SARS-CoV-2 spike protein polyclonal antibody (ThermoFisher Scientific, Invitrogen, PA5-81795) are used for demonstrating antigen-antibody based biosensor performance. The antibody has specificity for human SARS coronavirus spike S1 subunit protein, and cross-reactivity in ELISA and western blotting with SARS-CoV-2 (2019-nCoV) spike S1 and SARS-CoV-2 (2019-nCoV) spike receptor-binding domain (RBD). The binding of antibody to antigen was confirmed by western blotting (Figure 2). The selectivity of the sensor was studied by performing measurements with an alternate antigen: N4 bacteriophage protein, gp22, with a molecular weight of 15.9 kDa, that was mutated to N92A/22 and purified to near homogeneity. Deionised (DI) water was used for preparing dilutions, unless otherwise mentioned. PCB electrodes were designed using Autodesk EAGLE electronic design automation tool and were manufactured with conventional ENIG plating process (Circuit Systems (India) Ltd.). The ENIG process offered by this manufacturer results in formation of 75-100 nm gold on 3-5 µm nickel on 35 µm copper layer on the PCB.

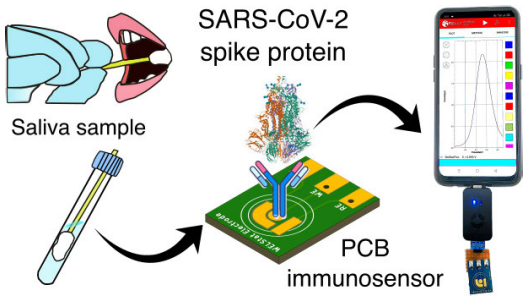

FIGURE 1. Illustration of use case for SARS-CoV-2 spike protein sensing in saliva enabled by low-cost immunosensor using ENIG PCB electrode presented in this work.

B. ELECTROCHEMICAL MEASUREMENTS

The voltammetry measurements were performed using PalmSens EmStat3 Blue and PalmSens Sensit Smart potentiostats. The potentiostat configuration and data acquisition are performed using PSTrace software and PSTouch Android app. Differential pulse voltammetry (DPV) measurements were performed using following settings: equilibration time = 8 s, voltage step = 3 mV, pulse voltage = 25 mV, pulse duration = 50 ms and scan rate = 20 mV/s. The potential (voltage) range is set as −0.05 V to +0.3 V. The equilibration time is the time during which the first

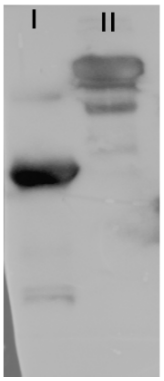

FIGURE 2. Western blot image for two different samples of SARS-CoV-2 spike protein antigen: (I) 1.7 mg/ml Fapon Biotech Inc. catalog ID FPZ0537, and (II) 4.7 mg/ml Meridian Life Sciences Inc. catalog ID 9556 (85 kDa), with SARS-CoV-2 spike protein polyclonal antibody (ThermoFisher Scientific, Invitrogen, PA5-81795). Sample (I) shows greater binding affinity with the antibody than sample (II).

potential of the measurement is applied to the electrochemical cell without recording the current. This is done in order to exclude initial capacitive current from interfering with the Faradaic current to be measured. Peak heights for DPV peak current were obtained using PSTrace software. The values for peak height obtained from PSTrace software were used for preparation of graphs wherever peak current values are discussed. The voltage corresponding to the peak current obtained in DPV is approximately identified with the polarographic half-wave potential and the peak height varies with the concentration of the analyte [38]. Cyclic voltammetry (CV) measurements were performed to confirm the deposition of cysteamine and glutaraldehyde on the electrodes. The measurements are configured using PSTrace software with following settings: equilibration time = 8 s, voltage range = −0.2 V to 0.5 V, scan rate = 100 mV/s and voltage step = 3 mV. The corrosion of the electrodes was assessed through electrochemical characterization (Tafel plot). To obtain the Tafel plot, and therefore the corrosion current density (I_{corr}), we used Bio-logic SP-200 potentiostat, and followed the ASTM G59 standard. The measurements were performed using EC-Lab® software.

C. ELECTRODE CLEANING

We investigated two separate methods of cleaning the electrodes. In the first method, the ENIG finish PCB electrodes were first wiped with IPA and then sonicated (ultrasonic cleaner, Equitron Medica Pvt. Ltd.) in absolute ethanol for 20 min. Electrodes cleaned with this method are referred to as EC (ethanol cleaned) electrodes in this paper. In the second method, the cleaning procedure was performed in three steps: (i) the electrodes are wiped with IPA, (ii) then sonicated in acetone, ethanol and DI water (1:1:1) for 20 min, and (iii) then the electrodes are wiped with lint free cloth and then again sonicated in ammonium hydroxide (NH_4OH), hydrogen peroxide (H_2O_2) and DI water mixture (1:1:5) for 20 min. The electrodes cleaned with this second method are referred to as AC (ammonium hydroxide cleaned) electrodes in this paper. After cleaning, the reference electrode (RE) is manually coated with Ag/AgCl paste using a paintbrush, and the electrodes are baked in an oven at 80 °C for 15 min to dry the paste.

D. ELECTRODE FUNCTIONALIZATION

Figure 3 shows an illustration of the process flow used to functionalize the electrodes (i.e. immobilization of antibodies) for bioanalyte (antigen) detection. 20 µl of 10 mM cysteamine solution prepared in absolute ethanol is dispensed on the working electrode. Next, 10 µl of 2.5 % glutaraldehyde solution prepared in DI water is dropcasted on the working electrode. The electrode is kept undisturbed for 2.5 h. Glutaraldehyde is a cross linking agent that covalently combines with cysteamine -NH_2, with the free end binding to the amino group of antibody [39], [40]. Excess glutaraldehyde is then rinsed with DI water. This is followed by immobilization of antibody on the glutaraldehyde layer. To prepare the antibody and antigen dilutions in phosphate buffered saline (PBS), 1X filtered PBS is prepared with 137 mM NaCl, 2.7 mM KCl, 10 mM Na_2HPO_4 and 1.8 mM KH_2PO_4. 12 µl of 10 µg/ml SARS-CoV-2 spike protein polyclonal antibody dilution prepared in PBS is dropcasted on the working electrode atop the glutaraldehyde layer. The electrode is then kept undisturbed at 4 °C for 12 h, and then rinsed with DI water to remove excess antibodies. To block the unbound surface on the electrode, 7 µl of 1 % BSA is dispensed on the working electrode, following which the electrode is kept undisturbed at 4 °C for 3 h. Thereafter the electrode is rinsed with DI water to remove excess BSA, and then stored at 4 °C until required for performing measurements. SARS-CoV-2 recombinant spike protein dilutions are prepared in PBS and artificial saliva, and stored at −20 °C until required for performing measurements.

III. RESULTS

A. OPTIMIZATION OF REDOX PROBE AND ELECTRODE CLEANING

To determine the appropriate KCl concentration to be used with the redox probe (potassium ferricyanide or potassium ferrocyanide), samples with various concentrations of KCl (50 mM, 100 mM, 200 mM and 300 mM) and potassium ferricyanide (2 mM, 4 mM, 8 mM and 16 mM) are prepared. Figure 4(a) shows optical micrographs of electrodes before and after performing DPV measurements, wherein each electrode was measured with all concentrations of $K_3Fe(CN)_6$ sequentially in decreasing order of concentration, for a given concentration of KCl. Each DPV measurement is obtained by dispensing 5 µl of the redox probe on the electrode. Four electrodes are used, one for each concentration of KCl. While the DPV voltammograms show decreasing trend with lower $K_3Fe(CN)_6$ concentration (Figure 4(b)), the optical micrographs clearly show that more corrosion is observed when higher concentration of KCl is used.

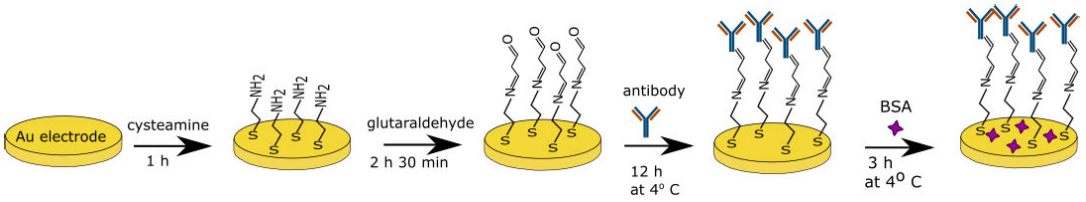

FIGURE 3. Illustration of electrode functionalization process flow.

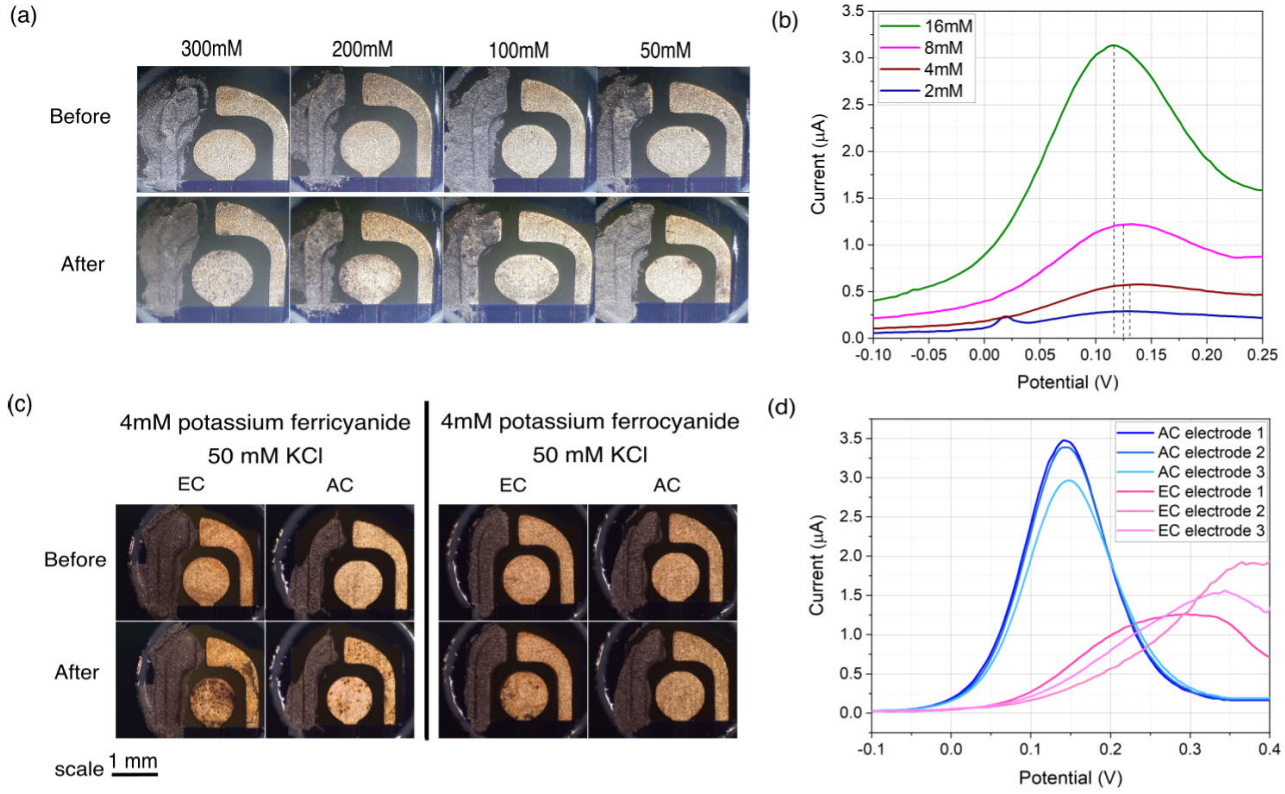

FIGURE 4. (a) Optical micrographs of electrodes measured using redox probes comprising of different concentrations of KCl, with decreasing concentration of potassium ferricyanide (16 mM, 8 mM, 4 mM and 2 mM) sequentially. (b) DPV voltammograms obtained for various concentration of potassium ferricyanide measured sequentially in decreasing order of concentration (with 50 mM KCl), on a single electrode. The peak current decreases with decrease in concentration of redox probe. (c) Potassium ferricyanide results in greater corrosion of the electrode surface than potassium ferrocyanide, after 10 successive measurements for the redox probe concentrations indicated in the figure. (d) DPV voltammograms (with 4 mM potassium ferrocyanide and 50 mM KCl) obtained on three electrodes each cleaned using EC and AC methods. The AC electrodes are more electroactive, yielding symmetrical and amplified DPV peaks as compared to EC electrodes.

ENIG finish PCB electrodes have mainly two types of surface defects: black pad and pinhole defects. These defects arise during the process of gold deposition through immersion in a solution containing gold salts, after the nickel layer is deposited on the copper layer. Due to presence of pinholes in the thin gold layer, the underlying copper layer is exposed [41], that in turn reacts with potassium ferricyanide resulting in corrosion of the electrode [42]. Note that electrode measured with 50 mM KCl also shows some trace of corrosion when $K_3Fe(CN)_6$ is used as redox probe (Figure 4(a)). Therefore, we investigated the impact of using potassium ferrocyanide ($K_4[Fe(CN)_6].3H_2O$) as redox probe on electrode corrosion. Figure 4(c) shows optical micrographs of electrodes captured before and after 10 successive DPV measurements for two redox probes: 4 mM potassium ferricyanide + 50 mM KCl, and 4 mM potassium ferrocyanide + 50 mM KCl. We observe that potassium ferrocyanide results in lesser corrosion as compared to potassium ferricyanide on EC as well as AC electrodes.

Conventional electrode cleaning recipes such as using piranha solution with reactive acids or several cycles of cyclic voltammetry with sulfuric acid at higher potentials [14], [15], [43] are not suitable for cleaning ENIG PCB electrodes, as they may cause striping of the thin gold layer on the electrode [44]. The $NH_4OH+H_2O_2$ mixture used in AC cleaning method is also called base piranha, and is a component in SC-1 cleaning used for removing organic impurities from silicon wafers. This mixture is a reactive oxidizer that removes all elemental carbon and organic impurities [45]. Sonication of electrodes in presence

of ethanol (EC electrode) does not effectively remove all impurities. The remaining impurities could react with the electrolyte and contribute to corrosion. On the contrary, the $NH_4OH+H_2O_2$ (AC) method is more effective in removing most of the impurities from the electrode surface. The superior performance of AC cleaning procedure as compared to EC is also visible in DPV voltammograms obtained using 4 mM potassium ferrocyanide and 50 mM KCl, as seen in Figure 4(d). The symmetry and amplification of the DPV current peak for AC electrodes indicate that the surface impurities are thoroughly removed and the electrode surfaces have become more electroactive.

To characterize the effect of redox probe on electrode corrosion, corrosion current density (I_{corr}) was measured by obtaining Tafel plots for three redox probes: (i) 4 mM potassium ferricyanide + 50 mM KCl, (ii) 4 mM potassium ferrocyanide + 50 mM KCl, and (iii) 2 mM potassium ferricyanide + 2 mM potassium ferrocyanide + 50 mM KCl on both EC and AC cleaned electrodes (Figure 5). In each measurement, 40 µl of the probe was dispensed on the cleaned electrode, and then the EC-Lab® software was used to obtain the Tafel plot, and perform curve-fit to determine I_{corr}. Figure 5 shows the Tafel plots obtained on one electrode each for all probes, for EC and AC cleaned electrodes. To find the I_{corr} value, the current (I) is plotted on X-axis (log scale) with working electrode potential (E) on Y axis, and the slopes of anodic current (β_a) and cathodic current (β_c), and corrosion potential (E_{corr}) value are measured with the help of linear fit performed in EC-Lab® software (visual aid shown in Figure 5(a)). The I_{corr} value is calculated in EC-Lab® software using the curve-fit for Stern relation:

$$I = I_{corr} \times \left(10^{\left(\frac{E-E_{corr}}{\beta_a}\right)} - 10^{\left(\frac{E-E_{corr}}{\beta_c}\right)} \right) \quad (1)$$

Table 1 presents the I_{corr} values obtained through these measurements. It is observed that potassium ferricyanide causes significantly larger corrosion of electrodes as compared to potassium ferrocyanide, consistent with the observations in Figure 4(c). The I_{corr} value for second AC cleaned electrode measured with potassium ferricyanide could not be measured due to excessive corrosion and damage of the electrode. All subsequent results reported in this paper are obtained with AC cleaned electrodes using potassium ferrocyanide as redox probe.

B. DETECTION OF SARS-CoV-2 SPIKE PROTEIN ANTIGEN

To facilitate easier handling of electrodes (i.e. selectively coat only the working electrode, and manual application of Ag/AgCl ink on reference electrode), we redesigned the electrodes such that the diameter of the circular WE is increased by a factor of 3 to 3 mm (Figure 6(a), photographs of electrodes shown before application of Ag/AgCl paste on RE). Figure 6(b) shows X-ray photoelectron spectroscopy (XPS) spectrum that confirms the deposition of cysteamine on the gold electrode surface through thiol-gold bond. The two sulfur peaks in the spectrum confirm the formation of

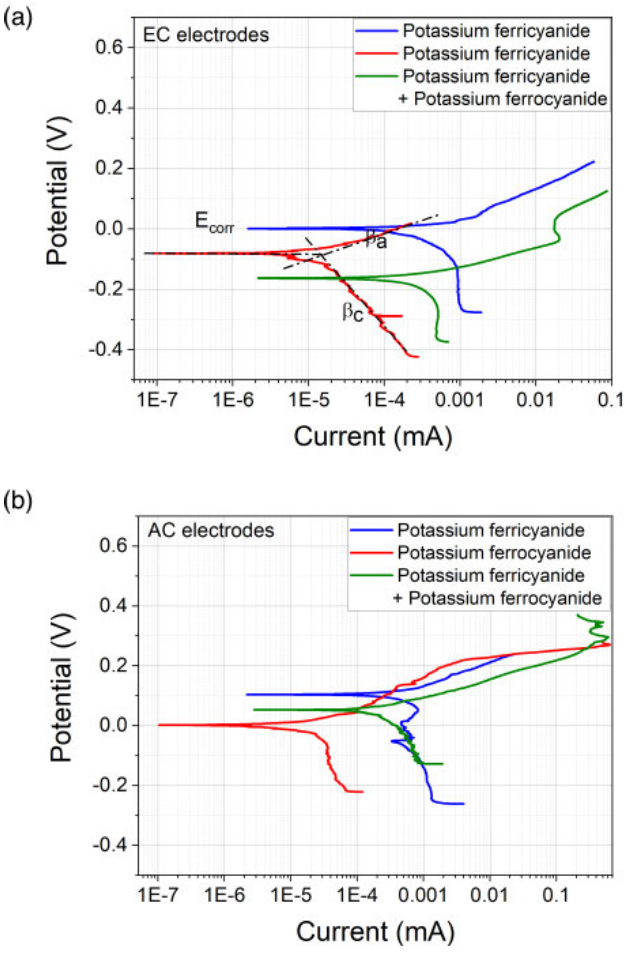

FIGURE 5. Tafel plots obtained for three different redox probes, on (a) EC electrodes (b) AC electrodes. The corrosion current density I_{corr} is the intersection of the anodic (β_a) and cathodic (β_c) slopes. Potassium ferricyanide results in significantly larger I_{corr} on these PCB electrodes.

TABLE 1. Corrosion current density (I_{corr} [$\mu A/cm^2$]) measured using Tafel plot for three different redox probes, on 2 electrodes each. The corrosion current density could be estimated for only one AC cleaned electrode with potassium ferricyanide, due to excessive corrosion and damage on the other electrode. The electrodes are not reused in these measurements.

Redox probe	EC		AC	
	1	2	1	2
4 mM potassium ferricyanide + 50 mM KCl	0.587	0.497	0.472	–
4 mM potassium ferrocyanide + 50 mM KCl	0.013	0.015	0.026	0.027
2 mM potassium ferricyanide + 2 mM potassium ferrocyanide + 50 mM KCl	0.361	0.415	0.437	0.295

thiol bond between cysteamine and gold electrode surface. To further confirm the deposition of cysteamine and glutaraldehyde on the electrode, CV measurement is performed (i) after AC cleaning, without modification, then (ii) after coating with cysteamine, and then (iii) after coating with glutaraldehyde (Figure 6(c)). It is observed that the peak current increases and the redox potential reduces slightly after coating cysteamine, consistent with observations made by

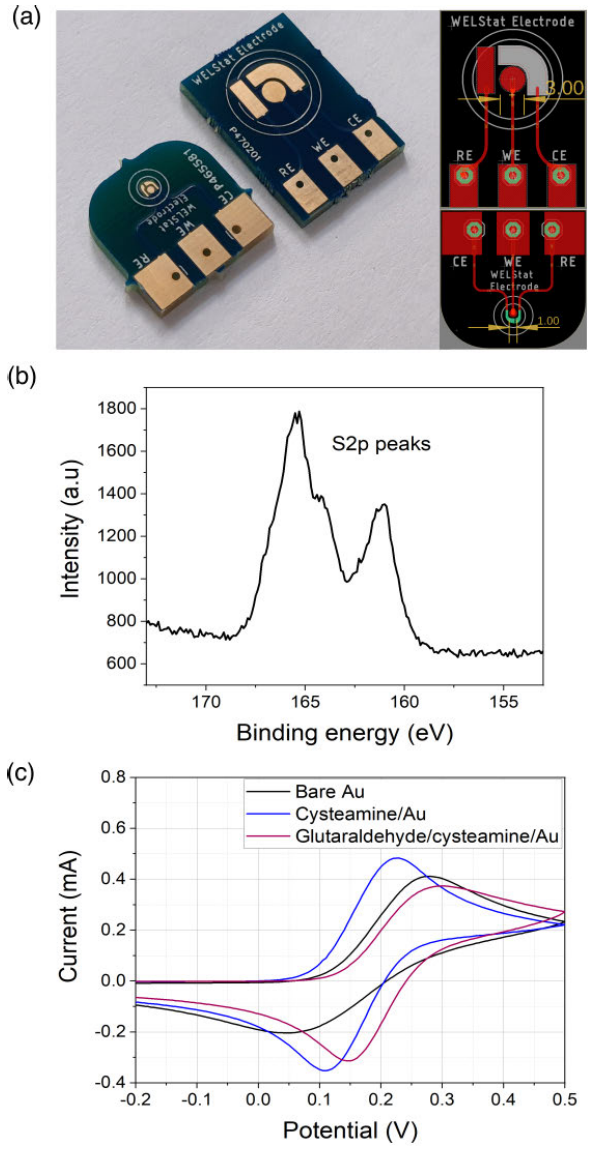

FIGURE 6. (a) Photograph of smaller ENIG finish PCB electrode, and redesigned larger electrode with 3 mm diameter working electrode. The photograph was taken prior to coating the reference electrode with Ag/AgCl paste. (Inset: schematics of electrodes, dimensions in mm.) (b) X-ray photoelectron spectroscopy (XPS) spectrum recorded after coating cysteamine on gold surface of the working electrode, confirming formation of thiol bond. (c) Cyclic voltammetry (CV) measurement obtained before and after coating cysteamine and glutaraldehyde on the bare PCB electrode.

Garyfallou *et al.* [21]. The peak current reduces significantly after coating glutaraldehyde due to formation of an insulating layer, consistent with observations made by Attar *et al.* [40].

The response of the biosensor to antigen-antibody interactions was studied by incubating spike protein antigen samples on the (Au/Cys/GA/spike-protein-Ab) modified PCB sensor sequentially in increasing order of concentration, and performing DPV measurement followed by rinsing of the electrode after measuring each concentration. The following sequence of measurements was followed: (i) First, 7 µl of the lowest concentration sample of antigen diluted in PBS was dispensed on the working electrode and the electrode

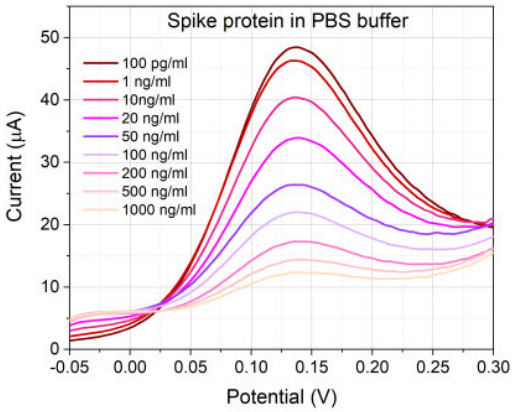

FIGURE 7. DPV voltammograms for SARS-CoV-2 spike protein antigen dilutions in PBS show reduction in peak current with increase in antigen concentration.

was kept undisturbed for 5 min. (ii) This was followed by rinsing the electrode with DI water and drying gently with a hand air blower. (iii) Thereafter, 120 µl redox probe (30 mM potassium ferrocyanide and 100 mM KCl) was dispensed on the electrode and DPV was recorded. (iv) The electrode was then rinsed with DI water and dried. (v) The process was repeated for the sample with next higher concentration of antigen on the same electrode. Representative DPV voltammograms for SARS-CoV-2 spike protein antigen dilutions in PBS measured on a modified electrode are shown in Figure 7. The DPV peak current decreases with increasing antigen concentration, due to inhibition of charge transfer by the insulating protein layer formed by antigen-antibody binding [46]–[48]. For measurements obtained on 4 electrodes each for SARS-CoV-2 spike protein dilutions prepared in PBS and artificial saliva (Figure 8(a)), it is observed that the (Au/Cys/GA/spike-protein-Ab) modified PCB sensor can detect spike protein in both PBS and saliva. The measurements were normalized i.e. percentage change in DPV peak current for each antigen concentration as compared to DPV peak current for 0.1 ng/ml antigen concentration, were compared for all electrodes. These calibration curves for SARS-CoV-2 spike protein detection using positive control samples prepared in PBS and artificial saliva are represented using a semilog plot (i.e. plot of percentage change in current vs. natural logarithm of concentration), following the widely used practice of presenting calibration curves in literature [49], [50]. The positive control (antigen in PBS) results were compared with negative control (only PBS, no antigen) on (Au/Cys/GA/spike-protein-Ab) modified electrodes. The results are shown in Figure 8(b), with negative control readings obtained on two electrodes. The box plots for NC1 and NC2 in Figure 8(b) consist of first four data points taken with negative control on each electrode. It is observed that the sensor can distinguish spike protein with concentration as low as 10 ng/ml from negative control. As seen in Figure 8(c), the magnitude of percentage change in DPV peak current values for SARS-CoV-2 spike protein in

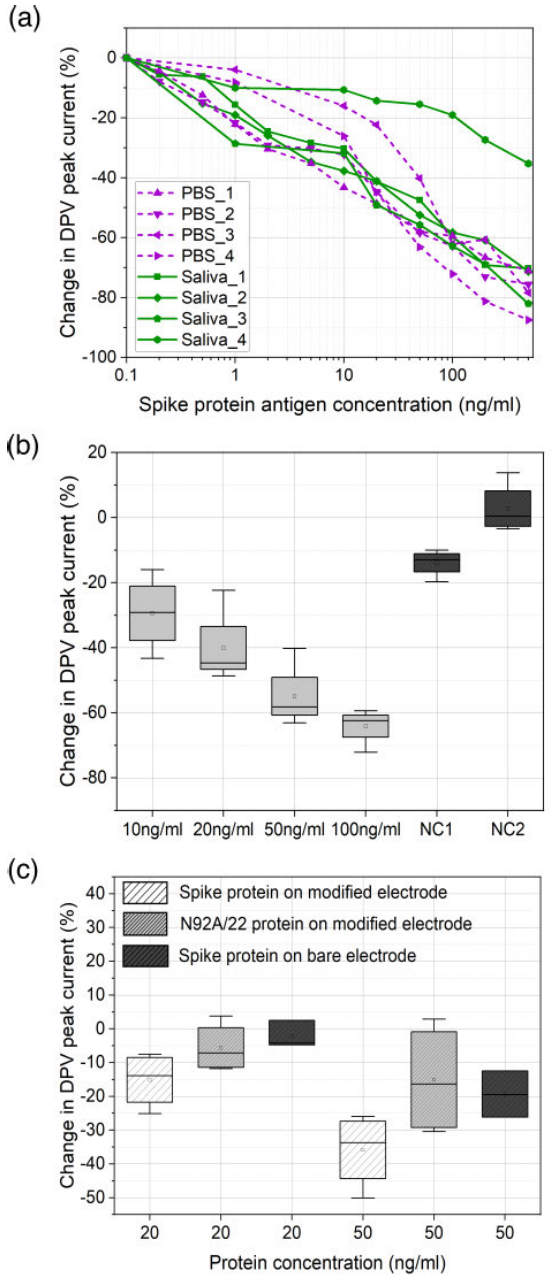

FIGURE 8. **(a) Change in DPV peak current measured for 4 electrodes each with SARS-CoV-2 spike protein dilutions in PBS and artificial saliva. (b) Change in peak current for positive controls (SARS-CoV-2 spike protein in PBS) are much larger than negative controls (PBS without spike protein). (c) Magnitude of percentage change in DPV peak current values (with respect to DPV peak current measured for 10 ng/ml antigen dispensed on electrode) for SARS-CoV-2 spike protein in PBS measured on modified (i.e. functionalised) electrodes and bare (i.e. AC cleaned, but unmodified) electrodes, and N92A/22 protein in PBS on modified electrodes.**

PBS measured on 4 (Au/Cys/GA/spike-protein-Ab) modified electrodes are significantly higher than measurements on 3 bare (i.e. AC cleaned, but unmodified) electrodes. The bare electrodes do not undergo processing with BSA, and may therefore be susceptible to adsorption of the antigen on the electrode surface. The change in peak height is lesser for bare electrodes as compared to modified electrodes due to antigen-antibody binding in the latter. The selectivity of the immunosensor is presented by comparison of the results to change in DPV current values for N92A/22 protein with 4 modified electrodes, that are comparable to the change in DPV current with bare electrodes, indicating that the modified electrode is more sensitive to SARS-CoV-2 spike protein antigen.

IV. DISCUSSION

Table 2 presents a comparison of this work with other PCB based biosensors reported in literature and Table 3 presents a comparison of this work with other low-cost electrochemical immunosensors for SARS-CoV-2 reported in literature. The primary advantage of antigen-antibody based immunosensors such as the one presented in this work, is significantly reduced measurement times as compared to enzyme-linked immunosorbent assay (ELISA), or polymerase chain reaction (PCR) based DNA sensing. The measurements reported in this work required only 5 min incubation of antigen with the antibody immobilized on the electrode. While the electrode functionalization process was manually performed in this work, the process requires a series of drop-casting and incubation steps, and is therefore amenable to batch processing. Moreover, the ENIG finish PCBs undergo no pre-processing (e.g. gold electroplating) other than the SC-1 cleaning process, and therefore the method presented here could be leveraged to realize extremely low cost of manufacturing for such immunosensors.

While a successful proof-of-concept immunosensor demonstration for SARS-CoV-2 spike protein antigen detection with ENIG PCB electrodes is demonstrated in this work, there are challenges that require further development. The main challenge in developing an immunosensor with ENIG finish PCBs thus far has been the presence surface defects in the thin gold layer on the electrode and susceptibility to corrosion. The cleaning and functionalization recipes presented here alleviate these issues and make these electrodes attractive candidates for low-cost immunosensors. Methods such as evaporation or sputtering of an additional thin layer of gold may be explored to address pinholes on the ENIG electrode surface, as a lower cost option compared to hard gold plating. As seen in Figure 8(a), it is evident that the electrode-to-electrode variability is an issue that needs to be addressed before considering such platforms for application-specific packaging and controlled trials. The relative standard deviation (RSD) of measurements shown in Figure 8(a) for 100 ng/ml and 500 ng/ml of spike protein antigen for results shown in are 7.4 % and 8.5 % respectively. The outlier (Saliva_4) is not included in RSD calculation. The variability could be attributed to surface defects, manual processes involved in deposition of cysteamine and glutaraldehyde, and Ag/AgCl coating on RE, manual method of dispensing sample and performing measurements etc. In future work, we aim to develop automated methods for coating the electrodes (e.g. screen printing, dip coating) and dispensing samples during measurements. We also seek to further study

TABLE 2. Comparison of this work with other PCB based biosensors reported in literature.

Reference	PCB gold finish	Cleaning	Surface modification	Application
Dutta et al. [7]	Electroplated	SC-1	SAM (3-mercaptopropoinic acid)	Glucose
Anastasova et al. [11]	ENIG (lower sensitivity), hard gold plating	H_2SO_4 CV	Au nanoparticles, electrodeposition, PEDOT, IrOx	Na^+, K^+, H^+
Kassanos et al. [13]	ENIG	H_2SO_4 CV	Au electroplating/ Pt nanoparticles/ electropolymerized phenol red	Glucose
Nandakumar et al. [51]	Electroplated	H_2SO_4 CV	Mercaptohexadecanoic acid (MDHA) / EDC	Bacterial contamination
Bhavsar et al. [52]	Electroplated	Stored in PBS	Mercaptohexadecanoic acid (MDHA) / EDC	Cytokine immunosensor
Alhans et al. [53]	Electroplated	Not reported	Carbon nantotubes (CNT) / GOx	Glucose
Evans et al. [54]	Electroplated	Not reported	Cysteine	Tuberculosis
Jacobs et al. [55]	Electroplated	Not reported	ZnO nanostructured thin film/DSP	Troponin
This work	ENIG	SC-1	Cysteamine/ glutaraldehyde	SARS-CoV-2 spike protein

TABLE 3. Comparison of this work with other low-cost electrochemical immunosensors for SARS-CoV-2 reported in literature.

Reference	Substrate	Surface modification	Target analyte	Lowest reported concentration
Li et al. [29]	Screen printed gold electrode, PET/PMMA microfluidic chip	Thiolated capture antibodies (cAbs)	SARS-CoV-2 nucleocapsid protein	$0.23\,ng/ml$
Vezza et al. [30]	Hard gold PCB	PFDT/ ACE2	SARS-CoV-2 spike protein	$1.68\,ng/ml$
Yakoh et al. [33]	Paper with screen printed graphene oxide electrodes	EDC/NHS	SARS-CoV-2 spike protein	$1\,ng/ml$
Fabiani et al. [34]	Screen printed electrode (graphite, silver)	Carbon black, magnetic beads	SARS-CoV-2 spike (S) protein and nucleocapsid (N) protein	$19\,ng/ml$ (S), $8\,ng/ml$ (N)
Rahmati et al. [36]	Screen printed carbon electrode	Nickel hydroxide nanoparticles	SARS-CoV-2 antibodies (IgM/IgG)	$0.1\,fg/ml$
Rahmati et al. [37]	Screen printed carbon electrode	Cu_2O nanocubes	SARS-CoV-2 spike protein	$0.25\,fg/ml$
This work	ENIG PCB	Cysteamine/ glutaraldehyde	SARS-CoV-2 spike protein	$0.1\,ng/ml$

the corrosion susceptibility of these electrodes to various electrolytes and redox probes, and explore alternate surface processing methods using conductive polymers such as polyaniline on the electrode surface, to make these ENIG finish PCBs more corrosion resistant and potentially improve the reliability and stability of the sensor [56].

V. CONCLUSION

In conclusion, we have demonstrated a platform for realizing low-cost and high sensitivity immunosensors using ENIG finish PCBs as electrodes. Our work focused on development of robust cleaning and antibody immobilization recipes, demonstrated through detection of SARS-CoV-2 recombinant spike protein antigen using this platform. In comparison with reports of other PCB based biosensors that employ gold electroplating on the electrode surface, the sensor proposed in this manuscript utilizes the ENIG finish gold electrode directly for antibody immobilization. We characterized the corrosion of PCB electrodes and discussed the optimization of redox probe for realizing the immunosensor. We also discussed the importance of cleaning of the electrode surface and suggested a suitable cleaning method for ENIG PCB electrodes to make them more electroactive and less susceptible to corrosion. The ENIG PCB sensor platform presented here can not only be used as an immunosensor but also adapted for wide range of applications such as aptamer based DNA sensors, chemical sensors based on molecular imprinted polymers, volatile organic compound and gas sensors etc. With suitable development, the platform reported here could be explored for development of a breathalyzer to directly detect virus copies in exhaled breath [57].

ACKNOWLEDGMENT

The PCB electrode design and preliminary characterization of the electrochemical sensor was performed at the Wadhwani Electronics Laboratory (WEL), supported by a grant from Wadhwani Charitable Foundation (WCF). The authors thank Dr. Ashish Indani and Devraj Goulikar at Tata Consultancy Services (TCS) for providing antigen and antibody samples, Dr. Andrew C. Ward at the University of Strathclyde for insightful discussions, and Dr. Arathy Varghese, Maheshwar Mangat, and Mahesh Bhaganagare at IIT Bombay for assistance with preliminary experiments.

REFERENCES

[1] D. Moschou and A. Tserepi, "The lab-on-PCB approach: Tackling the μTAS commercial upscaling bottleneck," *Lab Chip*, vol. 17, no. 8, pp. 1388–1405, 2017.

[2] B. B. Narakathu, S. G. R. Avuthu, A. Eshkeiti, S. Emamian, and M. Z. Atashbar, "Development of a microfluidic sensing platform by integrating PCB technology and inkjet printing process," *IEEE Sensors J.*, vol. 15, no. 11, pp. 6374–6380, Nov. 2015.

[3] F. Güth, P. Arki, T. Löher, A. Ostmann, and Y. Joseph, "Electrochemical sensors based on printed circuit board technologies," *Proc. Eng.*, vol. 168, pp. 452–455, Jan. 2016.

[4] F. T. C. Moreira, M. J. M. S. Ferreira, J. R. T. Puga, and M. G. F. Sales, "Screen-printed electrode produced by printed-circuit board technology. Application to cancer biomarker detection by means of plastic antibody as sensing material," *Sens. Actuators B, Chem.*, vol. 223, pp. 927–935, Feb. 2016.

[5] D. Evans, K. Papadimitriou, N. Vasilakis, P. Pantelidis, P. Kelleher, H. Morgan, and T. Prodromakis, "A novel microfluidic point-of-care biosensor system on printed circuit board for cytokine detection," *Sensors*, vol. 18, no. 11, p. 4011, Nov. 2018.

[6] H. Shamkhalichenar, C. J. Bueche, and J.-W. Choi, "Printed circuit board (PCB) technology for electrochemical sensors and sensing platforms," *Biosensors*, vol. 10, no. 11, p. 159, Oct. 2020.

[7] G. Dutta, A. Regoutz, and D. Moschou, "Commercially fabricated printed circuit board sensing electrodes for biomarker electrochemical detection: The importance of electrode surface characteristics in sensor performance," *Proceedings*, vol. 2, no. 13, p. 741, Nov. 2018.

[8] D. Moschou, T. Trantidou, A. Regoutz, D. Carta, H. Morgan, and T. Prodromakis, "Surface and electrical characterization of Ag/AgCl pseudo-reference electrodes manufactured with commercially available PCB technologies," *Sensors*, vol. 15, no. 8, pp. 18102–18113, Jul. 2015.

[9] S. A. Lim and M. U. Ahmed, "Electrochemical immunosensors and their recent nanomaterial-based signal amplification strategies: A review," *RSC Adv.*, vol. 6, no. 30, pp. 24995–25014, Mar. 2016.

[10] A. Wright. (2021). Printed circuit board surface finishes—Advantages and disadvantages. EPEC Build to Print Electronics. Accessed: Jul. 12, 2021. [Online]. Available: https://www.epectec.com/articles/pcb-surface-finish-advantages-and-disadvantages.html

[11] S. Anastasova, P. Kassanos, and G.-Z. Yang, "Multi-parametric rigid and flexible, low-cost, disposable sensing platforms for biomedical applications," *Biosensors Bioelectron.*, vol. 102, pp. 668–675, Apr. 2018.

[12] A. Accogli, A. Lucotti, and L. Magagnin, "*In situ*-Raman spectroscopy and electrochemical characterization on electroless nickel immersion gold process," *ECS Trans.*, vol. 75, no. 34, pp. 1–6, Jan. 2017.

[13] P. Kassanos, S. Anastasova, and G.-Z. Yang, "A low-cost amperometric glucose sensor based on PCB technology," in *Proc. IEEE SENSORS*, Oct. 2018, pp. 1–4.

[14] H. Wan, Q. Sun, H. Li, F. Sun, N. Hu, and P. Wang, "Screen-printed gold electrode with gold nanoparticles modification for simultaneous electrochemical determination of lead and copper," *Sens. Actuators B, Chem.*, vol. 209, pp. 336–342, Mar. 2015.

[15] T. Lee, Y. Lee, S. Y. Park, K. Hong, Y. Kim, C. Park, Y.-H. Chung, M.-H. Lee, and J. Min, "Fabrication of electrochemical biosensor composed of multi-functional DNA structure/Au nanospike on micro-gap/PCB system for detecting troponin I in human serum," *Colloids Surf. B, Biointerfaces*, vol. 175, pp. 343–350, Mar. 2019.

[16] E. Yorganci and E. Akyilmaz, "Alkaline phosphatase based amperometric biosensor immobilized by cysteamine-glutaraldehyde modified self-assembled monolayer," *Artif. Cells, Blood Substitutes, Biotechnol.*, vol. 39, no. 5, pp. 317–323, Oct. 2011.

[17] M. Wirde, U. Gelius, and L. Nyholm, "Self-assembled monolayers of cystamine and cysteamine on gold studied by XPS and voltammetry," *Langmuir*, vol. 15, no. 19, pp. 6370–6378, Sep. 1999.

[18] S. Kaur and I. Kaur, "Self-assembly of p-aminothiophenol on gold surface: Application for impedimetric and potentiometric sensing of cobalt (II) ions—A comparative study," *Electroanalysis*, vol. 31, no. 12, pp. 2507–2517, Dec. 2019.

[19] M. Zhou, L. Han, D. Deng, Z. Zhang, H. He, L. Zhang, and L. Luo, "4-mercaptobenzoic acid modified silver nanoparticles-enhanced electrochemical sensor for highly sensitive detection of Cu^{2+}," *Sens. Actuators B, Chem.*, vol. 291, pp. 164–169, Jul. 2019.

[20] P. Pandey, A. Pandey, and N. K. Shukla, "Screen printed gold electrode with cysteamine and single walled carbon nanotubes for the recognition of prostate specific antigen," *Mater. Today*, vol. 5, no. 7, pp. 15311–15318, 2018.

[21] G.-Z. Garyfallou, O. Ketebu, S. Şahin, E. B. Mukaetova-Ladinska, M. Catt, and E. H. Yu, "Electrochemical detection of plasma immunoglobulin as a biomarker for Alzheimer's disease," *Sensors*, vol. 17, no. 11, p. 2464, 2017.

[22] F. Arduini, S. Guidone, A. Amine, G. Palleschi, and D. Moscone, "Acetylcholinesterase biosensor based on self-assembled monolayer-modified gold-screen printed electrodes for organophosphorus insecticide detection," *Sens. Actuators B, Chem.*, vol. 179, pp. 201–208, Mar. 2013.

[23] G. Dutta, A. A. Jallow, D. Paul, and D. Moschou, "Label-free electrochemical detection of S. Mutans exploiting commercially fabricated printed circuit board sensing electrodes," *Micromachines*, vol. 10, no. 9, p. 575, Aug. 2019.

[24] Q. V. Bui, N. D. Nam, J. W. Yoon, D. H. Choi, A. Kar, J. G. Kim, and S. B. Jung, "Effect of gold on the corrosion behavior of an electroless nickel/immersion gold surface finish," *J. Electron. Mater.*, vol. 40, no. 9, pp. 1937–1942, Sep. 2011.

[25] M. S. Kumar, R. Nandeshwar, S. B. Lad, K. Megha, M. Mangat, A. Butterworth, C. W. Knapp, M. Knapp, P. A. Hoskisson, D. K. Corrigan, A. C. Ward, K. Kondabagil, and S. Tallur, "Electrochemical sensing of SARS-CoV-2 amplicons with PCB electrodes," *Sens. Actuators B, Chem.*, vol. 343, Sep. 2021, Art. no. 130169. [Online]. Available: https://www.sciencedirect.com/science/article/pii/S0925400521007383

[26] M. Barlev-Gross *et al.*, "Spike vs nucleocapsid SARS-CoV-2 antigen detection: Application in nasopharyngeal swab specimens," *Anal. Bioanal. Chem.*, vol. 413, pp. 1–10, Mar. 2021.

[27] A. Gowri, N. A. Kumar, and B. S. S. Anand, "Recent advances in nanomaterials based biosensors for point of care (PoC) diagnosis of COVID-19—A minireview," *TrAC Trends Anal. Chem.*, vol. 137, Apr. 2021, Art. no. 116205.

[28] M. Fani, M. Zandi, S. Soltani, and S. Abbasi, "Future developments in biosensors for field-ready SARS-CoV-2 virus diagnostics," *Biotechnol. Appl. Biochem.*, vol. 68, pp. 1–5, Aug. 2020.

[29] J. Li and P. B. Lillehoj, "Microfluidic magneto immunosensor for rapid, high sensitivity measurements of SARS-CoV-2 nucleocapsid protein in serum," *ACS Sensors*, vol. 6, no. 3, pp. 1270–1278, Mar. 2021.

[30] V. J. Vezza, A. Butterworth, P. Lasserre, E. O. Blair, A. MacDonald, S. Hannah, C. Rinaldi, P. A. Hoskisson, A. C. Ward, A. Longmuir, S. Setford, E. C. W. Farmer, M. E. Murphy, and D. K. Corrigan, "An electrochemical SARS-CoV-2 biosensor inspired by glucose test strip manufacturing processes," *Chem. Commun.*, vol. 57, no. 30, pp. 3704–3707, 2021.

[31] X. Peng, Y. Zhou, K. Nie, F. Zhou, Y. Yuan, J. Song, and J. Qu, "Promising near-infrared plasmonic biosensor employed for specific detection of SARS-CoV-2 and its spike glycoprotein," *New J. Phys.*, vol. 22, no. 10, Oct. 2020, Art. no. 103046.

[32] S. Mavrikou, G. Moschopoulou, V. Tsekouras, and S. Kintzios, "Development of a portable, ultra-rapid and ultra-sensitive cell-based biosensor for the direct detection of the SARS-CoV-2 S1 spike protein antigen," *Sensors*, vol. 20, no. 11, p. 3121, May 2020.

[33] A. Yakoh, U. Pimpitak, S. Rengpipat, N. Hirankarn, O. Chailapakul, and S. Chaiyo, "Paper-based electrochemical biosensor for diagnosing COVID-19: Detection of SARS-CoV-2 antibodies and antigen," *Biosensors Bioelectron.*, vol. 176, Mar. 2021, Art. no. 112912.

[34] L. Fabiani, M. Saroglia, G. Galatà, R. De Santis, S. Fillo, V. Luca, G. Faggioni, N. D'Amore, E. Regalbuto, P. Salvatori, G. Terova, D. Moscone, F. Lista, and F. Arduini, "Magnetic beads combined with carbon black-based screen-printed electrodes for COVID-19: A reliable and miniaturized electrochemical immunosensor for SARS-CoV-2 detection in saliva," *Biosensors Bioelectron.*, vol. 171, Jan. 2021, Art. no. 112686.

[35] W. Zeng, G. Liu, H. Ma, D. Zhao, Y. Yang, M. Liu, A. Mohammed, C. Zhao, Y. Yang, J. Xie, C. Ding, X. Ma, J. Weng, Y. Gao, H. He, and T. Jin, "Biochemical characterization of SARS-CoV-2 nucleocapsid protein," *Biochem. Biophys. Res. Commun.*, vol. 527, no. 3, pp. 618–623, 2020.

[36] Z. Rahmati, M. Roushani, H. Hosseini, and H. Choobin, "An electrochemical immunosensor using SARS-CoV-2 spike protein-nickel hydroxide nanoparticles bio-conjugate modified SPCE for ultrasensitive detection of SARS-CoV-2 antibodies," *Microchem. J.*, vol. 170, Nov. 2021, Art. no. 106718.

[37] Z. Rahmati, M. Roushani, H. Hosseini, and H. Choobin, "Electrochemical immunosensor with Cu_2O nanocube coating for detection of SARS-CoV-2 spike protein," *Microchim. Acta*, vol. 188, no. 3, pp. 1–9, Mar. 2021.

[38] F. Simões and M. Xavier, "6—Electrochemical sensors," in *Nanoscience and Its Applications* (Micro and Nano Technologies), A. L. Da Róz, M. Ferreira, F. de Lima Leite, and O. N. Oliveira, Eds. Norwich, NY, USA: William Andrew, 2017, pp. 155–178. [Online]. Available: https://www.sciencedirect.com/science/article/pii/B9780323497800000065

[39] F. López-Gallego, L. Betancor, C. Mateo, A. Hidalgo, N. Alonso-Morales, G. Dellamora-Ortiz, J. M. Guisán, and R. Fernández-Lafuente, "Enzyme stabilization by glutaraldehyde crosslinking of adsorbed proteins on aminated supports," *J. Biotechnol.*, vol. 119, no. 1, pp. 70–75, Sep. 2005.

[40] A. Attar, J. Mandli, M. M. Ennaji, and A. Amine, "Label-free electrochemical impedance detection of rotavirus based on immobilized antibodies on gold sononanoparticles," *Electroanalysis*, vol. 28, no. 8, pp. 1839–1846, Aug. 2016.

[41] A. T. Fiory, "Recent developments in rapid thermal processing," *J. Electron. Mater.*, vol. 31, no. 10, pp. 981–987, Oct. 2002.

[42] M. Kohn, "Some reactions of ferrocyanides and ferricyanides," *Anal. Chim. Acta*, vol. 3, pp. 297–299, 1949.

[43] A. Ferrario, M. Scaramuzza, E. Pasqualotto, A. De Toni, and A. Paccagnella, "Development of a disposable gold electrodes-based sensor for electrochemical measurements of cDNA hybridization," *Proc. Chem.*, vol. 6, pp. 36–45, 2012.

[44] A. Butterworth, E. Blues, P. Williamson, M. Cardona, L. Gray, and D. K. Corrigan, "SAM composition and electrode roughness affect performance of a DNA biosensor for antibiotic resistance," *Biosensors*, vol. 9, no. 1, p. 22, Feb. 2019.

[45] D.-H. Eom, G.-B. Lim, J.-G. Park, and A. A. Busnaina, "Reaction of ozone and H_2O_2 in NH_4OH solutions and their reaction with silicon wafers," *Jpn. J. Appl. Phys.*, vol. 43, no. 6R, p. 3335, 2004.

[46] J. Amani, A. Khoshroo, and M. Rahimi-Nasrabadi, "Electrochemical immunosensor for the breast cancer marker CA 15–3 based on the catalytic activity of a CuS/reduced graphene oxide nanocomposite towards the electrooxidation of catechol," *Microchim. Acta*, vol. 185, no. 1, p. 79, Jan. 2018.

[47] K. Kuntamung, P. Sangthong, J. Jakmunee, and K. Ounnunkad, "A label-free immunosensor for the detection of a new lung cancer biomarker, GM2 activator protein, using a phosphomolybdic acid/polyethyleneimine coated gold nanoparticle composite," *Analyst*, vol. 146, no. 7, pp. 2203–2211, 2021.

[48] K.-J. Huang, D.-J. Niu, W.-Z. Xie, and W. Wang, "A disposable electrochemical immunosensor for carcinoembryonic antigen based on nano-Au/multi-walled carbon nanotubes–chitosans nanocomposite film modified glassy carbon electrode," *Anal. Chim. Acta*, vol. 659, nos. 1–2, pp. 102–108, Feb. 2010.

[49] Q. Palomar, X. Xu, C. Gondran, M. Holzinger, S. Cosnier, and Z. Zhang, "Voltammetric sensing of recombinant viral dengue virus 2 NS1 based on Au nanoparticle–decorated multiwalled carbon nanotube composites," *Microchim. Acta*, vol. 187, no. 6, pp. 1–10, Jun. 2020.

[50] R. B. Clark and J. E. Dick, "Electrochemical sensing of perfluorooctanesulfonate (PFOS) using ambient oxygen in river water," *ACS Sensors*, vol. 5, no. 11, pp. 3591–3598, Nov. 2020.

[51] V. Nandakumar, D. Bishop, E. Alonas, J. LaBelle, L. Joshi, and T. L. Alford, "A low-cost electrochemical biosensor for rapid bacterial detection," *IEEE Sensors J.*, vol. 11, no. 1, pp. 210–216, Jan. 2011.

[52] K. Bhavsar, A. Fairchild, E. Alonas, D. K. Bishop, J. T. La Belle, J. Sweeney, T. L. Alford, and L. Joshi, "A cytokine immunosensor for multiple sclerosis detection based upon label-free electrochemical impedance spectroscopy using electroplated printed circuit board electrodes," *Biosensors Bioelectron.*, vol. 25, no. 2, pp. 506–509, Oct. 2009.

[53] R. Alhans, A. Singh, C. Singhal, J. Narang, S. Wadhwa, and A. Mathur, "Comparative analysis of single-walled and multi-walled carbon nanotubes for electrochemical sensing of glucose on gold printed circuit boards," *Mater. Sci. Eng., C*, vol. 90, pp. 273–279, Sep. 2018.

[54] D. Evans, K. I. Papadimitriou, L. Greathead, N. Vasilakis, P. Pantelidis, P. Kelleher, H. Morgan, and T. Prodromakis, "An assay system for point-of-care diagnosis of tuberculosis using commercially manufactured PCB technology," *Sci. Rep.*, vol. 7, no. 1, pp. 1–10, Dec. 2017.

[55] M. Jacobs, S. Muthukumar, A. P. Selvam, J. E. Craven, and S. Prasad, "Ultra-sensitive electrical immunoassay biosensors using nanotextured zinc oxide thin films on printed circuit board platforms," *Biosensors Bioelectron.*, vol. 55, pp. 7–13, May 2014.

[56] A. Korent, K. Ž. Soderžnik, S. Šturm, and K. Ž. Rožman, "A correlative study of polyaniline electropolymerization and its electrochromic behavior," *J. Electrochem. Soc.*, vol. 167, no. 10, Jun. 2020, Art. no. 106504.

[57] G. Giovannini, H. Haick, and D. Garoli, "Detecting COVID-19 from breath: A game changer for a big challenge," *ACS Sensors*, vol. 6, no. 4, pp. 1408–1417, Apr. 2021.

RUCHIRA NANDESHWAR received the Bachelor of Engineering degree in electronics and telecommunication from the Rajiv Gandhi College of Engineering and Research, Nagpur, India, in 2014, and the Master of Technology degree in microelectronics from the Indian Institute of Information Technology, Allahabad, India, in 2017. She is currently pursuing the Ph.D. degree with the Department of Electrical Engineering, IIT Bombay, specializing in solid state devices. Her research interests include electrochemical and colorimetric optical biosensors. Her work on colorimetric sensor for arsenic detection in water samples was selected as a Joint Winner of the 2020 Anveshan Design Fellowship organized by Analog Devices India Private Ltd. She received the Best Student Paper Award at 2018 IEEE Sensors Conference for her work on colorimetric sensor for myeloperoxidase.

M. SANTHOSH KUMAR received the master's degree from Bangalore University. He is currently pursuing the Ph.D. degree with the Molecular Virology Laboratory, Department of Biosciences and Bioengineering, IIT Bombay. He is working on elucidating the specific role of proteins involved in viral genome packaging. He is also interested in developing a viral gene-editing technique using CRISPR. He has worked on the development of instrumentation methodology for the detection of endotoxins.

KIRAN KONDABAGIL received the Ph.D. degree in biochemistry from CSIR-CFTRI, University of Mysore. His postdoctoral work at The Catholic University of America and Purdue University led to an understanding of the atomic details of viral genome packaging machinery and genome packaging mechanism. He is currently a Professor with the Department of Biosciences and Bioengineering, IIT Bombay. His research interests include the origin and evolution of viruses, molecular mechanisms of DNA packaging, replication, and repair in double-stranded DNA viruses, and detection and isolation of novel viruses from the environment.

SIDDHARTH TALLUR received the B.Tech. degree in electrical engineering from IIT Bombay, in 2008, and the M.S. and Ph.D. degrees in electrical and computer engineering from Cornell University, in 2011 and 2013, respectively. He is currently an Associate Professor with the Department of Electrical Engineering, IIT Bombay, and a Faculty-in-Charge of the Wadhwani Electronics Laboratory (WEL). Previously, he worked at Analog Devices Inc., Wilmington, MA, USA, from 2013 to 2016, as a MEMS Products and Applications Engineer. His research interests include high resolution and low cost physical and biosensors, high speed instrumentation, and embedded systems for sensing applications.